CONTENT

Karlo Kvaternik[1], Danijel Pavković[2], Josip Kasać[2], Mihael Cipek[2]

Comparison of Conventional and Fuzzy Logic-based Charging Control Systems without and with State-of-Charge Estimator

[1]AVL-AST d.o.o., Strojarska cesta 22, 10000 Zagreb, Croatia
[2]Faculty of Mechanical Engineering and Naval Architecture, University of Zagreb, Ivana Lučića 5, 10000 Zagreb, Croatia

Abstract

Lithium-titanate battery cells stand out among the various rechargeable lithium battery chemistries available today due to their exceptional thermal stability and operational safety, which make them suitable for highly demanding applications characterized by high charging/discharging rates and operating temperatures. This paper proposes a battery charging control system arranged in the so-called cascade control structure, wherein the battery voltage and state-of-charge control is performed by means of a fuzzy logic controller. An extended Kalman filter is used to provide the state-of-charge feedback utilizing the realistic nonlinear Thevenin model of the battery cell equivalent circuit. Simulations using a readily available lithium-titanate battery cell model demonstrate that fuzzy logic-based charging control reduces the time needed to recharge from deeply discharged state (from 20% state-of-charge initial value) by 17.7% compared to the conventional constant-current constant-voltage charging control strategy, with the average charging current used as the criterion for the comparison of these heterogenous control strategies.

***Keywords**: Lithium-Titanate Battery Cell; Constant-Current/Constant Voltage Charging; State-of-Charge Estimation; Extended Kalman Filter.*

1. Introduction

A comprehensive analysis conducted in [1] has revealed that approximately 20% of the global fossil fuel production is utilized by the transportation sector, leading to a significant contribution to greenhouse gas emissions. To enhance energy efficiency, reduce environmental impact, and decrease reliance on oil reserves, the electrification of the transportation sector has been advocated [2], wherein advanced battery technologies play a crucial role. It also proposed integrating the transport sector into the smart electricity grid paradigm, as later discussed in [3] for the case of road transport. The integration of the transport and energy sector into smart grids places particular demands on electric vehicle fleets, including the degree of electrification of the fleet, the cost of charging infrastructure and passenger capacity, as outlined in [4]. Monitoring the electric vehicle battery status during charging and discharging is crucial to ensure its prolonged service life, as shown in [5]. Battery energy storage technologies are also gaining traction in the railway transportation sector, with battery-hybridized locomotives and battery-electric locomotives offering advantages over conventional freight haul, as presented in [6].

Lithium secondary batteries are currently state-of-the-art electrochemical battery technology with favorable calendar life of up to 15 years and specific costs of about 145 EUR/kWh of stored electrical energy for the most advanced lithium titanate battery technology [7]. Presently the discharge power capacity of batteries is still significantly more favorable than that of alternative energy sources such as hydrogen fuel cells, especially when round-trip efficiency of energy conversion is considered [7]. The lithium-titanate oxide anode material has been proposed about a decade ago as a good replacement for commonly used carbon-based anodes in lithium-based secondary batteries due to the practical absence of anode material straining during high-rate discharging [8]. In fact, lithium titanate oxide may also be used as anode material in other, alternative battery chemistries such as those based on sodium-ion technology, which might be cheaper to manufacture due to the natural abundance of sodium as a raw material [9]. Moreover, lithium-titanate (LTO) batteries are considered as one of the safest available battery energy storage technologies, characterized by exceptional thermal stability, power density, cycle life and overall durability [10]. Hence, this battery production technology is likely to witness a significant growth in the

foreseeable future, wherein increased production volumes would likely bring down the overall production costs [11].

The key advantages of LTO battery cells are also discussed in [11], with additional benefits in terms of improved thermal material properties compared to other lithium-ion chemistries. These advantages lead to improved safety features, such as significant reduction of formation of dendrites and lithium plating of electrodes, even under harsh operating conditions, such as high current rates (about 25C for continuous discharging and charging), along with exceptional operational durability (20000 charging/discharging cycles with 1C current rate). The study presented in [11] concludes that LTO battery cells offer exceptional charging/discharging rate capabilities, albeit with reduced energy density compared to classical lithium-ion cells with graphite anodes. Due to their exceptional cycling characteristics and durability LTO cells appear to be well suited for hybrid power applications in electrified vehicle powertrains. Thus, extensive research has been carried out in the available literature regarding the innovative LTO cell technologies and charging characteristics [12], state-of-charge (SoC) estimation [13], state-of-health (SoH) estimation [14] and advanced control techniques [15], including those for stationary energy storage use in solar photovoltaic systems [16] and mobile applications such as those in heavy-duty vehicles [17].

Recent research in battery modeling and estimation has shown that the Thevenin equivalent circuit models are effective for modeling and estimation of the battery state-of-charge (SoC) for lithium-ion batteries in electric vehicles (EVs) [18, 19]. Simulation and experimental results have validated the accuracy of these models in predicting battery behavior under different operating conditions [18, 19], and ongoing research is directed towards exploring the general applicability of these relatively straightforward models for estimating the SoC of battery packs, which is crucial for the safe and efficient operation of electric vehicles (EVs) [20]. The electrolyte polarization dynamics within the Thevenin model can either be modeled as a first-order RC parallel term [19] or the more general second-order RC model [18], wherein the former is typically used as a trade-off in terms of simplicity compared to the more accurate second-odder polarization dynamics model. Using the equivalent circuit models within the improved extended Kalman filter algorithm has been proposed to enhance the accuracy of SoC estimation in lithium-ion batteries [21]. On the other hand, a hybrid estimator combining the extended Kalman filter (EKF) and sliding mode observer has been demonstrated to improve the robustness of SoC estimation in the presence of disturbances [22]. In fact, such advanced SoC estimation techniques, i.e. those relying on sigma point Kalman filter, long short-term memory neural networks, convolution neural networks, and different hybrid methods, have been reviewed for possible utilization in battery management systems (BMS), with a focus on reducing average error and improving performance in EV applications [23]. In particular, the development of advanced BMS is crucial for improving battery performance, safety, and longevity in EVs [23, 24]. BMS features include charging/discharging control, precise monitoring, heat management, battery safety, and protection, as well as accurate SoC estimation [23, 24]. Recent research has focused on the comprehensive analysis and comparison of charging control methods for lithium-ion battery packs, classifying them as non-feedback-based, feedback-based, and intelligent charging methods [25]. A good review of the advancements and difficulties in cutting-edge battery technology and cutting-edge BMS for EVs can be found in [26].

Efficient charging of rechargeable batteries is contingent upon the charger's circuit design and control strategy which performs three essential functions: (i) commencing the charging process, (ii) controlling the charging rate and battery terminal voltage for optimal charging performance, and (iii) terminating the charging upon completion, determined by a suitable end-of-charging criterion [24]. However, batteries typically exhibit notable terminal voltage nonlinear behavior during charging [27, 28]. This may be challenging from the standpoint of precise battery SoC tracking [29], which is key for preventing battery overcharging and related cell aging and SoH deterioration [30]. For that reason, battery SoC needs to be monitored throughout the charging process by an appropriate estimator, such as the EKF [29], which has been successfully employed in [31] to augment the conventional constant-current constant-voltage (CCCV) charging system, ultimately resulting in about 25% speed up of the charging process. Battery charging techniques (charging control strategies) can be categorized in many ways. According to [24], the charging strategies can be categorized as non-feedback based (or open-loop) strategies, feedback-based, and intelligent charging strategies, whereas reference [32] breaks down the charging strategy types into so-called simple (or traditional) charging strategies, optimized charging strategies based on different optimized current waveforms to achieve the charged state and the model-based charging strategies.

In traditional (conventional) battery charging applications, the so-called CCCV charging technique (see e.g. [24]) is usually preferred when recharging the battery from the discharged state [32], while the so-called float-charge maintenance or trickle charging approaches [33] are usually reserved for maintaining the battery charge once it has been fully charged. The main advantage of the CCCV approach is that the charging current and battery terminal voltage are effectively limited by means of respective battery controllers [27], and it can also find use in fast charging applications [34]. Also, it has been considered as a good benchmark for other more sophisticated charging control strategies to be compared against [24]. Moreover, its relative simplicity and virtual independence on the sophisticated internal battery model [32], currently make it the one of the most widely used charging strategies [33]. However, batteries typically exhibit notable terminal voltage nonlinear behavior during charging [28]. This may be challenging from the standpoint of precise battery SoC tracking [29], which is key for preventing battery overcharging and related cell aging and SoH deterioration [30]. For that reason, battery SoC needs to be monitored throughout the charging process by an appropriate estimator, such as the extended Kalman filter [29], which has been successfully employed in [31] to augment the conventional CCCV charging system, ultimately resulting in about 25% speed up of the charging process. A good review of charging strategies for lithium-ion batteries can be found in [35].

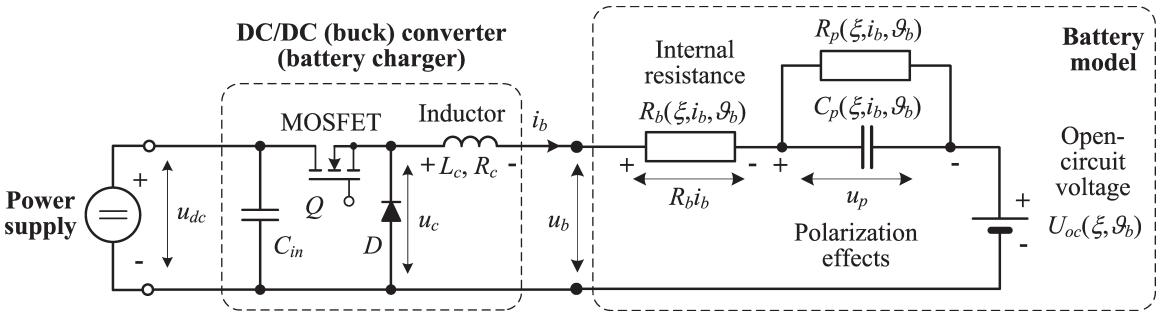

Fig. 1. Quasi-static battery equivalent electrical circuit model with charging power converter.

The implementation of sophisticated control strategies is anticipated to yield additional enhancements in both the duration of the charging process and the effectiveness of State of Charge (SoC) tracking. Among these, the optimization-based control strategies, such as the model-predictive control (MPC), may be particularly well-suited for solving multiple-criteria charging scenarios [35], such as those where battery temperature and current rate play a critical role regarding the battery SoH preservation [33]. Multistage constant current (MCC) represents a generalization of the traditional constant-current (CC) charging technique, wherein the duration of each constant-rate charging stage can either be SoC-dependent or battery terminal voltage dependent [34]. For example, the comparative study presented in [31] has pointed out that utilization of fuzzy logic control-based approach presented in [36] can yield about 13% speedup of the battery recharging, whereas MCC charging with offline optimization of the charging trajectory [37] and MPC with moving horizon estimation of the battery SoC [38], may result in relative charging process speedups of 17% and 30%, respectively. However, the latter charging algorithms can be numerically quite demanding due to requirement for charging trajectory optimization, whereas the fuzzy logic-based charging control strategy may be relatively easily implemented as a form of expert knowledge-based system utilizing the SoC estimator as a digital twin of the battery which aids the charging process (see [31]).

Several studies have investigated methods to preserve battery SoH during charging, such as the MPC approach that accounts for voltage and temperature constraints to reduce the battery stress during the charging process [39]. The study presented in [40] also focused on thermal effects, optimizing power and current profiles to balance the charging rate and temperature rise. Alternative charging profiles have shown promise as well, such as incorporating negative current pulses within the CCCV technique to improve battery SoH [41] and using a temperature-compensated model to enhance the charging speed within the CCCV charging strategy [42]. Moreover, MCC charging has been combined with the least mean squares estimation for faster charging in [43], while offline optimization, such as the genetic algorithm-based approach proposed in [44] and the dynamic programming utilized in [45] have also been explored to determine optimal charging sequences and minimize heat losses during charging.

Fast charging plays a vital role in alleviating range anxiety associated with battery electric vehicles and is a key element in promoting the widespread adoption of electric vehicles [46]. However, it also contributes to the accelerated aging of batteries [47].

Therefore, the study presented in [47] analyzed the impact of fast charging on lithium-ion batteries' aging using real-world driving cycles from European cities, considering different charger sizes and battery types, while the study conducted in [46] has evaluated different fast-charging strategies, considering their parameterization effort, battery type, and real-world applicability. In the context of fast charging, thermal management of lithium-ion batteries is essential for ensuring their safety, performance, and longevity in electric vehicles [48]. To this end, the study presented in [48] has provided a state-of-the-art review of recent advancements in lithium-ion battery thermal management strategies for high charge/discharge cycles.

Having in mind the advantageous features of LTO battery cells and the above-described aspects of battery charging control system design and performance indices, the motivation for this paper has been to design a charging strategy that can surpass the traditional CCCV charging approach while honoring the battery voltage and current constraints. The hypothesis of this paper is that using a fuzzy logic-based battery charging control strategy in conjunction with precise SoC estimation would result in notable charging process speedup without adverse effects to battery state-of-health associated with exceeding the charging current and terminal voltage. For that purpose, the fuzzy logic controller relies on battery SoC information provided by an EKF-based state estimator and readily available battery terminal voltage and current measurements, and it is subsequently compared to the conventional CCCV charging control strategy by means of simulations.

2. Battery cell model

A battery cell can be modeled by its equivalent electrical circuit model, shown on the left-hand-side in Fig. 1. The battery equivalent circuit model comprises a voltage source corresponding to the battery open-circuit voltage U_{oc}, electrolyte polarization effects modeled by an equivalent parallel RC circuit (with resistance R_p and capaci-

tance C_p parameters) and an equivalent series resistance R_b [31]. The above model results in the following voltage u_b vs. current i_b relationship in the Laplace s-domain:

$$u_b(s) - U_{oc}(s) = i_b(s)R_b + \frac{R_p i_b(s)}{\tau_p s+1}, \qquad (1)$$

where $\tau_p = R_p C_p$ is the polarization time constant.

All parameters of the above model may depend on battery temperature ϑ_b, battery current i_b and state-of-charge ξ, which is defined in the following manner:

$$\xi = \frac{1}{Q_b(I_b)} \int i_b dt, \qquad (2)$$

with battery charge capacity Q_b also depending on the average battery current load I_b, and the magnitude of these charge capacity variations depending on the battery type and chemistry [49].

The right-hand-side of Fig. 1 shows the principal schematic of the basic battery charging system featuring a buck DC/DC power converter and a battery cell represented by its equivalent electrical circuit model. The buck converter topology comprises the active (switching) element (power MOSFET transistor Q) feeding the inductor (characterized by its inductance L_c and resistance R_c) and parallel-connected freewheeling diode D. The semiconductor switch (MOSFET) modulates the DC supply voltage by means of high-frequency pulse-width modulation (PWM) thus providing the power converter output voltage u_c with adjustable magnitude and fast dynamics (negligible voltage delay).

The main advantage of the equivalent circuit model is that the battery parameters (internal resistances, polarization time constant, open-circuit voltage characteristic) that are characteristic for individual battery types can be experimentally obtained by means of suitable battery tests conducted for the anticipated operating modes (battery SoC and charging/discharging currents) and stored as parameter maps (look-up tables). In that sense, the battery charging control system and SoC estimator design can be easily adapted to the battery type in question by conducting battery model identification experiments and updating the battery parameter maps (see [31] and references therein). The above state-of-charge and current dependent parameters of the equivalent electrical circuit model (the so-called Thevenin model) of a commercial 30Ah/2.4V/6C lithium titanate battery cell [50] have been experimentally estimated using an appropriate experimental setup as described in [51].

The battery open-circuit voltage curve is recorded by using constant-current charging tests, wherein the experiment is characterized by periodic short-duration battery charging intervals followed by at least two-hour long recuperation and battery voltage settling periods. Experimental results are shown in Fig. 2a, and they have been interpolated by cubic splines to obtain a smooth (differentiable) static curve. The battery charge capacity vs. average discharging current curve has also been reconstructed based on constant-current discharging tests, and the resulting cubic spline-interpolated battery capacity vs. discharging current characteristic $Q_b(I_b)$ is shown in Fig. 2b (note that the charge capacity curve for currents below 6 A is obtained by extrapolation). The particular LTO battery cell is characterized by a relatively small decrease of its charge capacity Q_b with the discharging current I_b that amounts to less than 5% for the considered range of discharging current values (i.e. from 6A to 24 A). For both characteristics the interpolation (and extrapolation in the case of static curve in Fig. 2b) has been performed over 1001 samples of the static characteristic look-up table inputs.

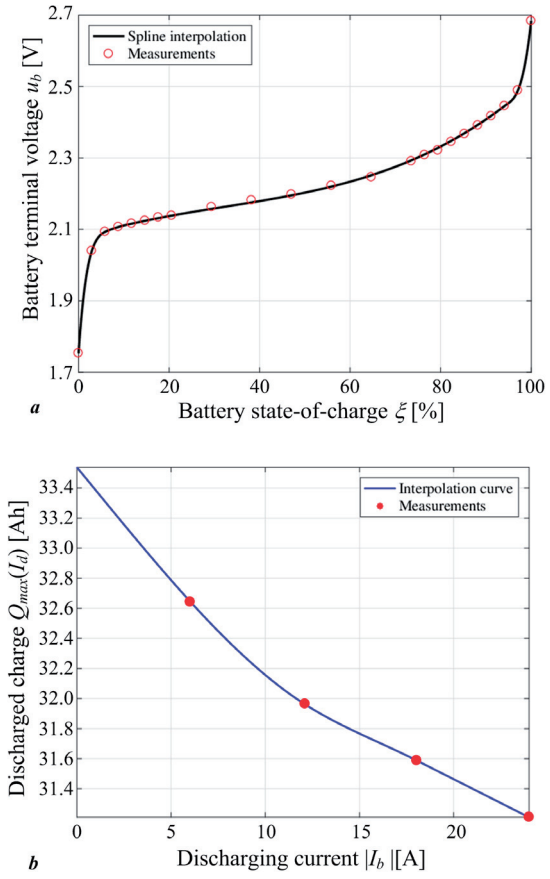

Fig. 2. Lithium-titanate battery cell charge capacity vs. average current characteristic (a) and battery charge capacity vs. current dependence (b).

Recording the battery equivalent circuit model parameter maps with respect to battery state-of-charge and battery current has been carried out by using off-line least squares identification technique [52] on the results of previously recorded battery charging and discharging tests under a pseudo-random binary sequence (PRBS) signal excitation, as explained in [52]. Figure 3 shows the two-dimensional maps of the battery equivalent circuit (Thevenin model) parameters recorded for the considered 30 Ah / 2.4 V LTO battery cell, wherein the battery series resistance R_b and polarization resistance exhibit rather low values over the middle of the state-of-charge range, but their values tend to increase when the battery cell is being fully discharged ($\xi \to 0$) or fully charged ($\xi \to 100\%$). The polarization time constant τ_p takes on values between 2 s and 12 s and is dependent on the charging/discharging current and battery state-of-charge (Fig. 3c).

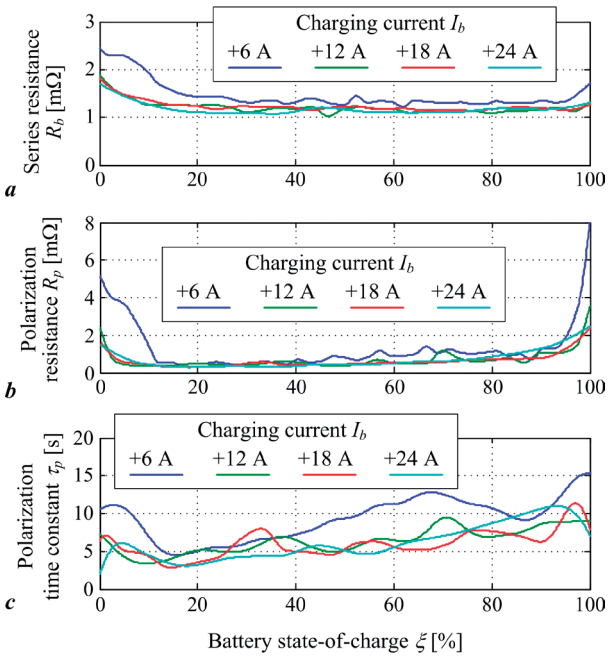

Fig. 3. Equivalent series resistance (a) polarization resistance (b) and polarization time constant (c) vs. SoC for different charging rates.

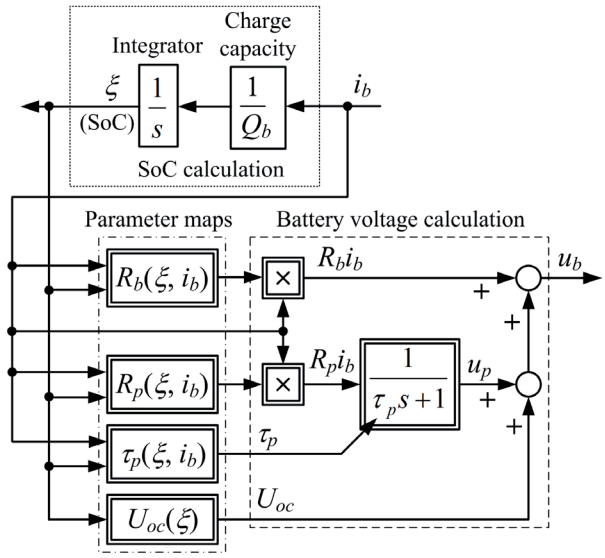

Fig. 4. Block diagram of battery equivalent circuit model.

The estimated parameters of the battery equivalent electrical circuit are used to build the battery simulation model, wherein the battery current is used as model input. Fig. 4 shows the current-input quasi-static battery model with state-of-charge ξ and polarization voltage u_p treated as model state variables. The battery terminal voltage equation $u_b = R_b i_b + U_{oc} + u_p$ is implemented by using the identified battery parameter static maps $R_b(\xi, i_b)$, $R_p(\xi, i_b)$, $\tau_p(\xi, i_b)$ and $U_{oc}(\xi)$ as shown in Fig. 4. The overall simulation model and the above parameter static maps are implemented within the MATLAB/Simulink software environment, with the above parameter maps implemented either as two-dimensional look-up tables (R_b, R_p, τ_p) or a one-dimensional look-up table (U_{oc}). To facilitate high-precision of the battery cell model during simulations, the dynamic equations within the simulation model are solved by using the variable-step ODE45 solver (a medium-order method for non-stiff equations), with relative and absolute tolerances of 10^{-3} and 10^{-6}, respectively.

It should be noted that the second-order RC model can be generally more accurate in capturing the more complex aspects of battery polarization voltage dynamics, as shown in [20] where the second-order RC network polarization voltage model has been identified based on the battery current step response characteristic. In contrast, the first-order RC model of polarization voltage dynamics used herein has been identified by using the auto-regressive model with exogenous inputs (ARX model) and least-squares identification technique [51], which primarily identified the dominant dynamics of the polarization voltage model. More precisely, the less dominant dynamic modes have been shown to exhibit very fast response dynamics (typically much less than the identification data sampling time $T = 1$s used in [51]), which has been attributed to the numerical error of the LS-based parameter estimation technique. One way of dealing with this problem would have been to utilize the battery model identification methodology presented in [20], but that would be beyond the scope of this work.

3. Charging control systems and state-of-charge estimator

This section outlines the design of the benchmark CCCV control system based on battery voltage PI controller and the fuzzy logic-based battery charging controller, along with the design of the EKF-based SoC estimator.

3.1. Charging control systems

Figure 5 shows the control system structure for constant-current/constant voltage (CCCV) battery charging based on the inner current control loop (assumed to embedded within the charging DC/DC power converter) with battery terminal voltage limiting outer feedback loop featuring a proportional-integral (PI) feedback controller. This type of charging control system may be considered a state-of-the-art benchmark case. In this so-called cascade control system arrangement, the inner current control loop receives the current reference i_{bR} as a sum of the maximum charging current I_{max} used during the constant-current stage of the charging process and the negative current command i_{blim} from the superimposed voltage limiting controller, which is activated when the battery terminal voltage measurement u_{bs} exceeds the battery voltage limit value u_{blim} (dead-zone block in Fig. 5). The main advantage of the CCCV approach is that the charging current and battery terminal voltage are effectively limited by means of respective battery controllers, thus reducing battery thermal stresses and preventing battery over-voltages [27]. In

particular, the battery current limit can be preset to the recommended battery charging current value obtained from battery manufacturers' data, whereas the battery voltage limit is typically set to the open-circuit voltage (OCV) value corresponding to 100% battery state-of-charge [27]. In that way, the CCCV charging control system can be easily adapted to different battery types, each characterized by different recommended charging current values and end-of-charge battery voltages. The detailed procedure for voltage PI controller tuning is presented in [31]. The comprehensive analysis presented therein has shown such control strategy results in battery terminal voltage asymptotically reaching the desired open-circuit voltage value $U_{oc}(\xi_R)$ related to the desired state-of-charge target ξ_R as the battery charging current i_b approaches zero in the final, constant-current phase of the charging process.

Fuzzy logic is commonly found in expert systems, wherein the expert knowledge can be represented in the form of linguistic IF-THEN relationships or linguistic rules [53]. Block diagram in Figure 6 shows the fuzzy logic-based battery charging control system comprising a fuzzy controller with two feedback variables: battery SoC difference $\Delta\xi$ (control error) and battery terminal voltage. Membership functions $\mu_i(\Delta\xi(k))$ and $\mu_j(u_b(k))$ and the output function values uch in the output set of the proposed fuzzy logic-based controller are shown in Fig. 7. In this application, smoothed trapezoidal membership functions shapes are used in the inference part of the controller, as shown in Figs. 7a and 7b. There are four membership functions associated with SoC difference (Fig. 7a): high SoC difference (red dashed curve), medium SoC difference (black dash-dotted curve), low SoC difference (blue dash-dotted curve), and near-zero SoC difference (green solid curve). The latter membership function and its associated linguistic rule basically determine the end-of-charging behavior of the fuzzy logic controller, wherein the controller output should be lowered towards its minimum value which corresponds to the fully charged battery terminal voltage and zero-current conditions. On the other hand, there are three battery voltage-related membership functions (Fig. 7b) associated with low battery voltage (red dashed curve), medium battery voltage (black solid curve) and high battery voltage (blue dash-dotted curve), which, alongside the other SoC difference membership functions determine the charging behavior (fuzzy controller output, i.e. voltage command uc) when the battery is being charged. The output (inference) part of the fuzzy control law is of the Mamdani type (see [53]), and its input-output map uc is shown in Fig. 7c. It uses triangular output weighting functions (corresponding to fast charge, normal mode and end-of-charge) to assign appropriate power converter voltage command in relation to fuzzy controller input rules. Greater weight is assigned to SoC difference values in the mid-to-high range, and the voltage command u_c is also adapted with respect to battery terminal voltage to address possible violations of battery current limitations.

3.2. State-of-charge estimator

The battery equivalent circuit model identification results are used as a basis for battery state variable estimation, which, according to equations (1) and (2), translates to on-line estimation of battery polarization voltage and state-of-charge. Due to the non-linear nature of the battery model (i.e. it is characterized by non-linear parameter maps, as illustrated in Figs. 2 and 3), a suitable non-linear state estimator, such as the EKF [54] needs to be employed for this task.

The process model given by equations (1) and (2) is re-written in the matrix-vector state-space form and transformed into its discrete-time counterpart that can be used within the EKF-based state estimator [54]:

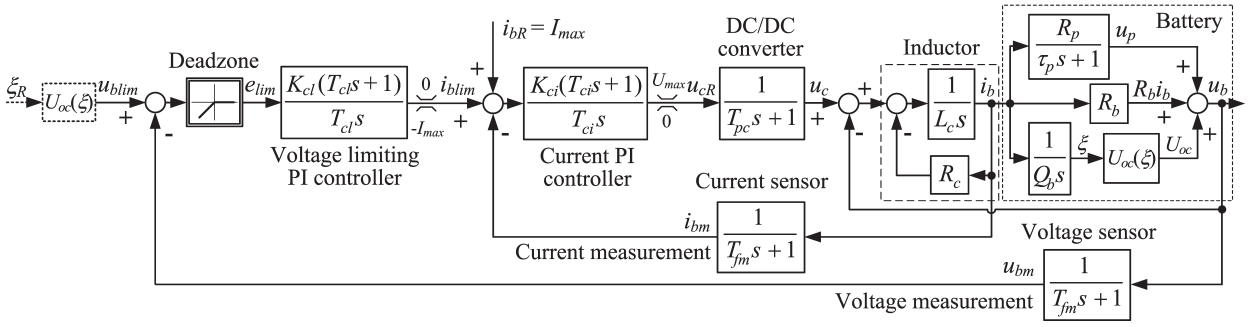

Fig. 5. Cascade control system arrangement for battery charging with battery terminal voltage limiting controller [31].

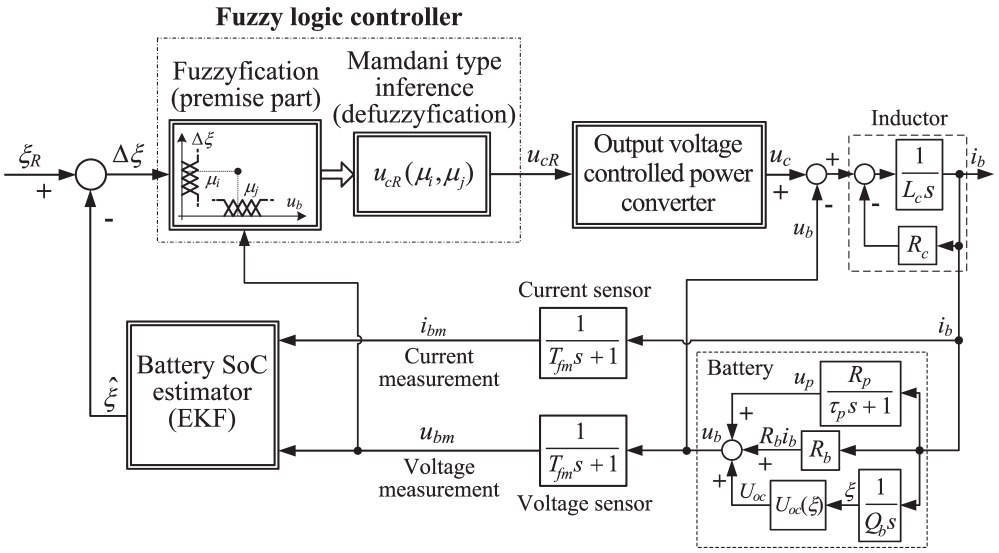

Fig. 6. Block diagram representation of fuzzy logic-based controller for battery charging utilizing SoC estimator and battery terminal voltage feedback.

$$\boldsymbol{x}(k) = \boldsymbol{f}(\boldsymbol{x}(k-1), i_{bm}(k-1)) + \boldsymbol{\Omega}\boldsymbol{v}(k), \tag{3}$$

$$u_{bm}(k) = \boldsymbol{h}(x(k), i_{bm}(k)) + e(k), \tag{4}$$

where u_{bm} and i_{bm} are battery voltage and current measurements, respectively (see Figs. 5 and 6), while the state variable vector $\mathbf{x}(k)$, the state perturbation covariance matrix $\mathbf{Q}$ and stochastic perturbation scaling matrix $\boldsymbol{\Omega}$ are defined as follows:

$$\boldsymbol{x}(k) = \begin{bmatrix} u_p(k) \\ \xi(k) \end{bmatrix}, \quad \boldsymbol{\Omega} = \begin{bmatrix} T & 0 \\ 0 & T \end{bmatrix}, \quad \boldsymbol{Q} = \begin{bmatrix} q_u & 0 \\ 0 & q_\xi \end{bmatrix}. \tag{5}$$

The block diagram representation of the EKF-based estimator is shown in Fig 8, with the nonlinear state-space model used within it to calculate the so-called a-priori state estimate $\hat{\boldsymbol{x}}(k|k-1)$, which is subsequently corrected via battery voltage measurement resulting in the final (a-posteriori) state estimate $\hat{\boldsymbol{x}}(k|k)$. For that purpose, the estimation algorithm needs to calculate the estimator correction gains based on the so-called Ricatti equation [54]. This process requires the calculation of the following Jacobian matrices, which are related to partial derivatives of all battery model parameters with respect to battery state-of-charge and polarization voltage (battery system states):

$$\boldsymbol{F}(k) = \frac{\partial \boldsymbol{f}(\hat{\boldsymbol{x}}, i_b)}{\partial \hat{\boldsymbol{x}}}\bigg|_{\substack{\hat{\boldsymbol{x}}(k-1|k-1), \\ i_b(k-1)}}, \tag{6}$$

$$\boldsymbol{H}(k) = \frac{\partial \boldsymbol{h}(\hat{\boldsymbol{x}}, i_b)}{\partial \hat{\boldsymbol{x}}}\bigg|_{\substack{\hat{\boldsymbol{x}}(k|k-1), \\ i_b(k)}}, \tag{7}$$

which are required to estimate the error covariance matrix $\mathbf{P}$ within the estimator by using the assumed variances of state perturbations $\boldsymbol{v}$ (characterized by the perturbation covariance matrix $\mathbf{Q}$ whose elements are chosen as a trade-off between estimator noise sensitivity and tracking ability) and the noise e variance r in the battery terminal voltage (measurement) u_b [55].

4. Simulation results

Figure 9 shows the results of the EKF-based SoC estimator subjected to the constant-current battery charging simulation scenario with battery current equal to 24 A. The results show rather good agreement between the state-of-charge obtained from the simulation model and the estimator in the estimator steady state (Fig. 9a), which points to favorable estimator tracking ability. Fig. 9b shows that the estimator is characterized by fast convergence towards the actual battery state-of-charge from the mismatched state, i.e. it can be tuned for rather fast and well-damped response. The state-of-charge estimator steady-state tracking error absolute value does not exceed 0.05%.

The proposed fuzzy logic-based battery charging control system has been verified against the voltage PI controller-based conventional charging control strategy [31] by means of simulations using the model of the LTO battery cell and the DC/DC (buck) power converter implemented within MATLAB/Simulink software environment, with power converter inductor modeled with inductance L_c = 0.7 mH, and series resistance R_c = 50 mΩ [31]. Since the fuzzy logic-based control strategy has different structure (i.e. it does not include the inner current control loop and associated charging current limit at the controller output) compared to the conventional voltage PI controller, it does not yield the constant-current/constant-voltage (CCCV) charging profile characterized by a rather long

constant-current (CC) charging interval followed by a relatively short constant-voltage (CV) charging interval as the voltage PI controller does [31]. Therefore, to compare these controllers in a straightforward way, the fuzzy logic-based control strategy is simulated first. The charging simulation scenario then utilizes the conventional (PI controller-based) control strategy whose charging current limit (which determines the constant current charging phase) is set to the average value of the charging current obtained by the fuzzy logic-based charging system. In this way, the charging current commanded by the PI controller during the CC charging interval would result in a similar amount of charge being stored within the battery as in the case of fuzzy logic-based charging controller with variable charging current profile. In both cases, the end of charging is indicated when the charging current drops below the minimum current value I_{min}, set in simulations to I_{min} = 10 mA.

Figure 10 shows the comparative results of the proposed fuzzy logic-based and conventional control strategy. The fuzzy logic-based control strategy initiates battery charging with relatively large currents by means of commanding the corresponding voltage reference to the voltage-controlled DC/DC power converter (see red traces in Figs. 10b and 10d), which is progressively increased until it reaches the recommended charging current value of 30 A which corresponds to the so-called 1C charging rate [50]. Large current rates are maintained in the middle of the SoC region corresponding to low values of battery series and polarization resistances (cf. traces in Figs. 10a and 10b). As the SoC increases towards the fully charged battery state, the charging current is progressively decreased by means of DC/DC power converter. Namely, throughout the charging process, the battery voltage steadily increases (Fig. 10c), and the fuzzy logic algorithm adjusts the DC/DC converter voltage command to decrease the current when the estimated SoC provided by the EKF-based estimator approaches the fully charged state, as well as to keep the battery terminal voltage within the prescribed limits [50]. The fuzzy logic-based control strategy has resulted in the total charging time of 5701 s, and the average changing current of about 20 A. The latter value has been used as the charging current limit (I_{max} = 20 A in the block diagram in Fig. 7) within the

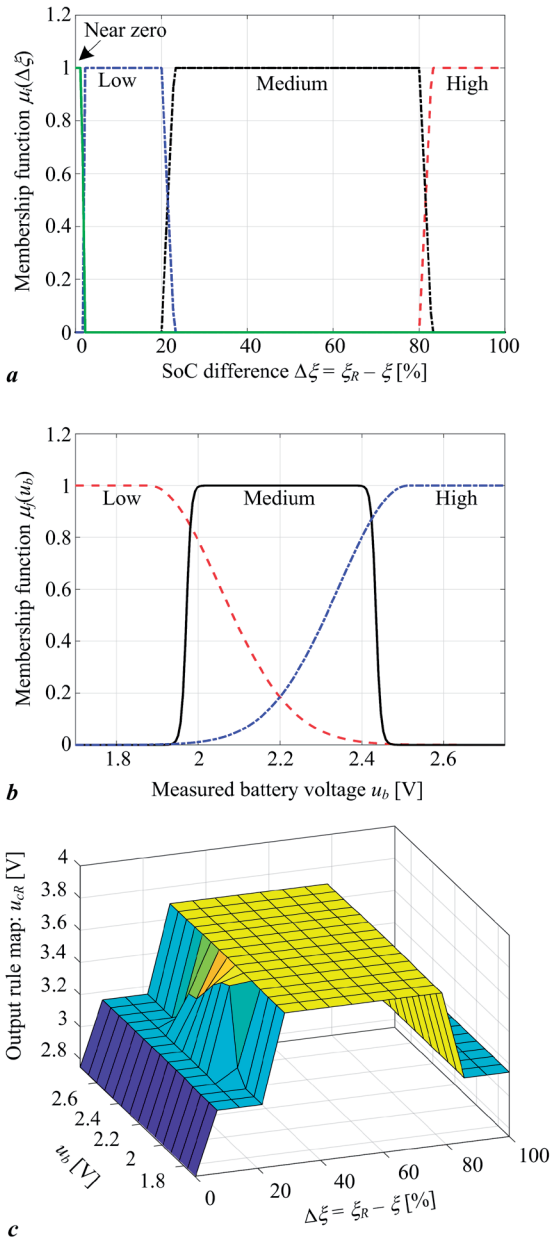

Fig. 7. Membership functions of fuzzy controller with respect to SoC control error signal (b) and battery terminal voltage signal (b), and output rule values (c).

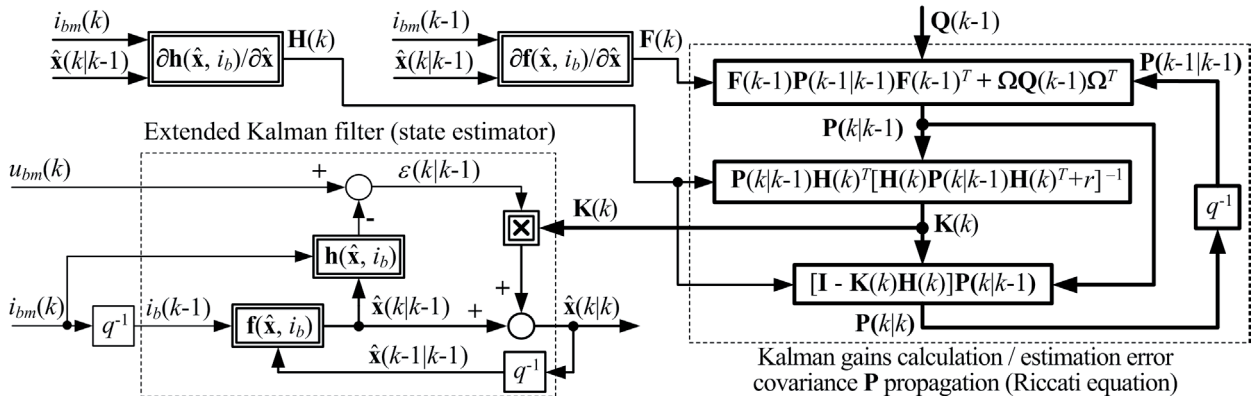

Fig. 8. Principal block diagram representation of extended Kalman filter for battery state-of-charge estimation.

conventional PI controller-based CCCV control strategy. The results in Fig. 10 show that the conventional CCCV control strategy is predominated by the constant-current regime throughout the charging process, with the constant voltage charging regime being only briefly active near the end of charging. This results in battery SoC increasing with constant slope, in contrast to the fuzzy logic-based strategy, wherein the SoC slope is variable, and adjusted with respect to the SoC operating point (Fig. 10a). The estimated SoC from the EKF estimator used as the fuzzy logic controller feedback is again very well matched with the actual battery SoC (see results in Fig. 9) which points to fast convergence and good tracking ability of the EKF-based estimator (cf. red solid trace and blue dashed trace in Fig. 10a). The conventional CCCV strategy results in the charging time of 6297 s. Consequently, the fuzzy logic-based control strategy has in fact achieved a 17.7% speedup compared to the conventional PI controller-based CCCV control strategy, while achieving nearly identical end-of-charging SoC value under these test conditions (Table 1).

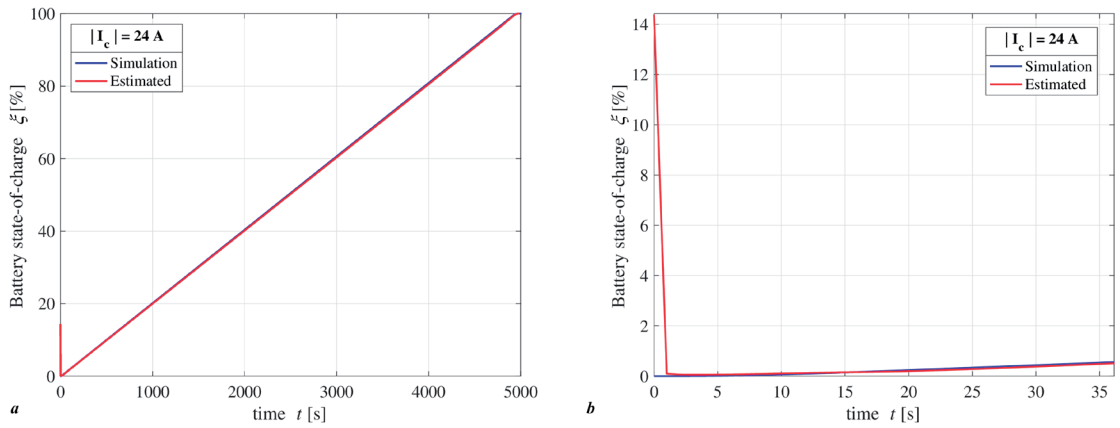

Fig. 9. Comparative EKF vs. battery simulation model responses during constant-current charging: overall results (a), and initial (transient) part of response from mismatched state (b).

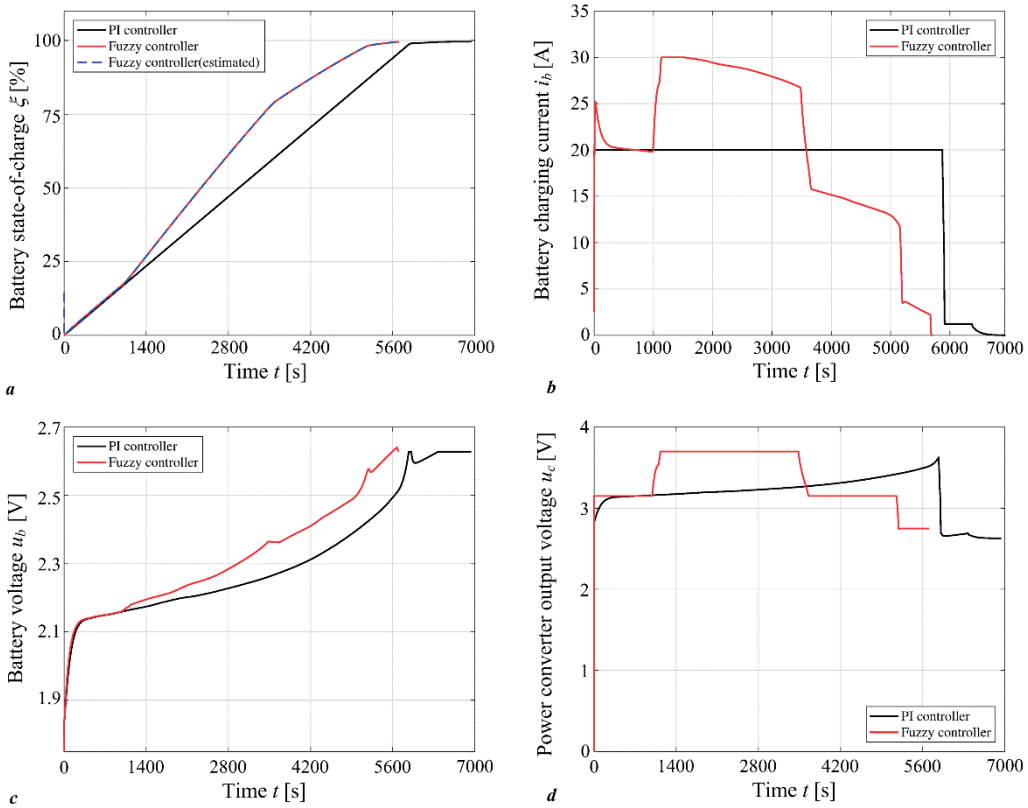

Fig. 10. Comparative simulation results of fuzzy controller-based and voltage PI controller-based battery charging systems: state-of-charge responses (a), charging current responses (b), battery terminal voltage trace (c) and DC/DC power converter output voltage traces (d).

As indicated in Fig. 10b, the CCCV charging strategy will try to maintain the constant charging rate practically until the battery terminal voltage reaches the target value, whereas the fuzzy controller (after the initial "boost" of the charging current) tends to gradually decrease the charging current before the end of charging occurs. The current profile effectively determines the battery heat losses due to series and polarization resistance ($P_t = i_b^2 R_s + u_p^2/R_p$), whose values tend to increase at higher SoC values (see Fig. 3). Figure 11 shows the profiles of battery model series and polarization resistance parameters R_b and R_p (Fig. 11a and 11b), heat dissipation losses P_t (Fig. 11c) and total generated heat $W_t = \int P_t dt$ (Fig. 11d). Simulation results show that the fuzzy controller resulting in higher battery charging currents indeed causes higher heat losses during the initial "boost" of battery current, but subsequently decreases the heat dissipation in the second part of the charging process, whereas the PI controller-based CCCV charging strategy tends to increase the heat losses towards the end of charging (Fig. 11c). Consequently, both charging strategies result in similar total generated heat at the end of charging, with the fuzzy controller-based charging generating only 7.1% larger amount of total waste heat compared with PI controller-based charging strategy (Fig. 11d). This points to similar performance of these control strategies with respect to battery heat losses, whereas the fuzzy controller-based charging strategy has been shown to be more effective with respect to battery charging time (see discussion related to Fig. 10). Thus, it may be inferred that utilization of fuzzy controller-based charging strategy may indeed be well suited for faster battery recharging, while also being characterized by similar end-of-charging battery temperature, which is directly related to the total waste heat generated during charging. In conclusion, the fuzzy logic-based charging strategy, even though being characterized by 17.7% shorter recharge time and higher charging rates, would have the same effect on heat losses-related battery aging effects and battery state-of-health, and would likely result in similar battery lifetime when compared to the conventional CCCV strategy which is typically used in practical applications.

The sampling time of the PI controller, fuzzy logic charging controller and the EKF-based state-of-charge estimator in the above simulation scenario have been set to $T = 1$ s (sampling frequency is 1 Hz), which is justified because the charging process and the dominant dynamics of the process model are rather slow. Since the sampling time is rather large, the target microcontroller operating at standard clock speeds should be able to perform the numerical calculations associated with the EKF estimator and the fuzzy logic-based controller algorithms, provided that it also possesses embedded floating point arithmetic functionality. One such example would be the ARM Cortex-M4 and Arm Cortex-M7 architectures [56], which also feature analog interfaces needed for battery measurement signals acquisition. An example of a development board that could be used for prototyping and testing such solutions within the open-source software environment would be the Arduino GIGA R1 [57].

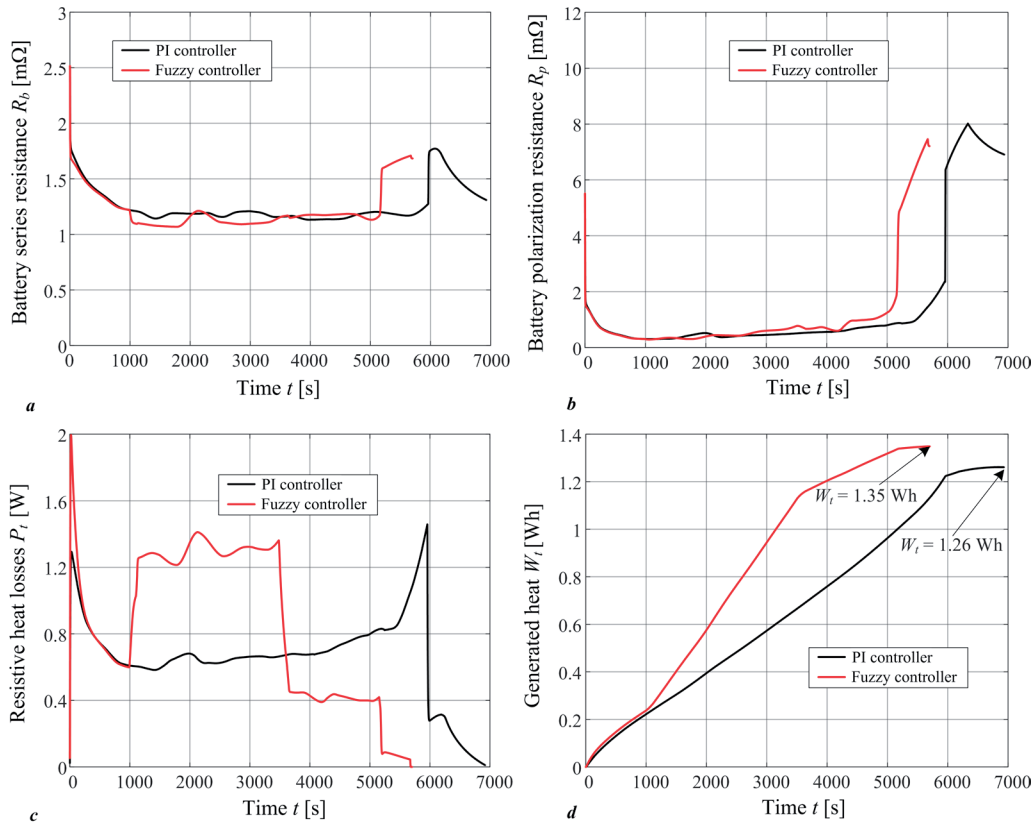

Fig. 11. Comparative simulation traces of battery series resistance (a), battery polarization resistance (b), resistive heat losses (c) and overall generated heat (d) during charging by means of conventional PI control and fuzzy logic control.

Table 1. Comparative results of conventional vs. fuzzy logic-based charging control strategy.

	Fuzzy controller	PI voltage controller
Charging time [s]	5701	6927
Final battery voltage [V]	2.6280	2.6283
Final battery SoC [%]	0.9950	0.9956

5. Conclusion

The paper has presented the results of simulation verification and benchmarking of the fuzzy logic-based charging control system with respect to the battery voltage PI controller-based conventional constant-current/constant voltage (CCCV) control strategy for a state-of-the-art lithium titanate (LTO) 30 Ah/2.4 V battery cell. For simulation verification of both control strategies, a dedicated equivalent electrical circuit simulation model of the LTO battery cell has been built based on the previously obtained experimental data. The results have indicated that the fuzzy logic-based charging controller can recharge the battery in a much shorter time compared to the conventional CCCV charging, while achieving approximately the same average charging current value.

The charging control system benchmark, i.e. the conventional battery terminal voltage PI controller-based system has been arranged in the co-called cascade control structure, with the superimposed PI controller commanding the current target to the DC/DC power converter with straightforward limitation of the battery charging current. In the case of fuzzy logic-based charging control, the fuzzy logic controller commands an appropriate voltage reference to the DC/DC power converter. The DC/DC converter voltage reference is determined based on the finite set of linguistic rules in the input (premise) part of the fuzzy control law, which determine the membership levels of battery state-of-charge tracking error and terminal voltage to corresponding input sets. Based on those membership levels, the output (inference) part of the fuzzy control law calculates the so-called "crisp" output value which corresponds to the DC/DC power converter voltage reference. In order to implement the fuzzy control law, a suitable battery state-of-charge estimator has been designed using the battery cell equivalent electrical circuit model and the extended Kalman filter (EKF) design methodology.

The proposed charging control strategies have been verified and compared within the MATLAB/Simulink software environment. The EKF-based estimator has been capable of accurately tracking the battery state-of-charge (SoC), while also being characterized by fast convergence. The fuzzy logic-based charging control system utilizing the additional estimated battery SoC feedback in combination with the battery terminal voltage feedback has shown distinct advantages over the conventional PI controller-based CCCV control strategy based on battery terminal voltage feedback. In particular, the fuzzy logic-based charging control system has achieved a 17.7% speedup of the charging process while honoring the battery terminal voltage and current limitations, which is primarily due to the additional degree of freedom with respect to battery charging current in the low-to-middle battery *SoC* operating regime, which the conventional CCCV charging strategy cannot take advantage of.

Future work is going to be directed towards further refinement of the fuzzy logic-based charging control system and its adaptation for the more general case of current-controlled DC/DC power converter, and state-of-health (SoH) aware adaptation aimed at minimizing battery stresses during charging. Further developments of suitable battery SoC/SoH estimators are also foreseen along with the experimental verification of the proposed fuzzy logic-based charging control system.

6. Acknowledgment

This research has been supported by the European Commission through the Horizon 2020 project "Maximizing the impact of innovative energy approaches in the EU islands" (INSULAE).

7. References

[1] McCollum, D., Krey, V., Kolp, P., Nagai, Y., & Riahi, K. (2014). Transport electrification: A key element for energy system transformation and climate stabilization. *Climate Change*, *(38)*, 651-664.

[2] Buzzonii, L., & Pede, G. (2012). New prospects for public transport electrification. In *Proceedings of International Conference on Electrical Systems for Aircraft, Railway and Ship Propulsion (ESARS 2012)*.

[3] Deur, J., Škugor, B., & Cipek, M. (2015). Integration of Electric Vehicles into Energy and Transport Systems. *Automatika - Journal for Control, Measurement, Electronics, Computing and Communications*, *(56)*, 395-410.

[4] Chinese, D., Pinamonti, P., & Mauro, C. (2021). A spatially explicit optimization model for the selection of sustainable transport technologies at regional bus companies. *Optimization and Engineering*, *(22)*, 1921-1954.

[5] Cipek, M., Pavković, D., Kljaić, Z., & Mlinarić, T.J. (2019). Assessment of Battery-Hybrid Diesel-electric Locomotive Fuel Savings and Emission Reduction Potentials based on a Realistic Mountainous Rail Route. *Energy*, *(173)*, 1154-1171.

[6] Cipek, M., Pavković, D., Krznar, M., Kljaić, Z., & Mlinarić, T.J. (2021). Comparative Analysis of Conventional Diesel-Electric and Hypothetical Battery-Electric Heavy Haul Locomotive Operation in terms of Fuel Savings and Emissions Reduction Potentials. *Energy*, *(232)*, 121097.

[7] Victoria, M., Zhu, K., Brown, T., Andresen, G.B., & Greiner, M. (2019). The role of storage technologies throughout the decarbonisation of the sector-coupled European energy system. *Energy Conversion and Management*, *(201)*, 111977.

[8] Sandhya, C.P., John, B., & Gouri, C. (2014). Lithium titanate as anode material for lithium-ion cells: a review. *Ionics*, *(20)*, 601–620.

[9] Liang, Z., Hui-Lin, P., Yong-Sheng, H., Hong, L., & Li-Quan, C. (2012). Spinel lithium titanate (Li4Ti5O12) as novel anode material for room-temperature sodium-ion battery. *Chinese Physics B*, *(21)*, 028201.

[10] Zhang, X., Peng, H., Wang, H., & Ouyang, M. (2018). Hybrid Lithium Iron Phosphate Battery and Lithium Titanate Battery Systems for Electric Buses. *IEEE Transactions on Vehicular Technology*, *(67)*, 956–965.

[11] Nemeth, T., Schröer, P., Kuipers, M., & Sauer, D.U. (2020). Lithium titanate oxide battery cells for high-power automotive applications – Electro-thermal properties, aging behavior and cost considerations. *Journal of Energy Storage*, *(31)*, 101656.

[12] Odziomek, M., Chaput, F., Rutkowska, A., Świerczek, K., Olszewska, D., Sitarz, M., Lerouge, F., & Parola, S. (2017). Hierarchically structured lithium titanate for ultrafast charging in long-life high-capacity batteries. *Nature Communications*, *(8)*, 15636.

[13] Song, C., Luo, J., Chen, X., & Peng, Z. (2023). SoC Estimation of Lithium Titanate Battery Based on Variable Temperature Equivalent Model. In S. Patnaik, R. Kountchev, Y. Tai, & R. Kountcheva (Eds.), *3D Imaging—Multidimensional Signal Processing and Deep Learning* (pp. 123-143). Smart Innovation, Systems and Technologies, Vol 349.

[14] Jenu, S., Hentunen, A., Haavisto, J., Pihlatie, M. (2022). State of health estimation of cycle aged large format lithium-ion cells based on partial charging. *Journal of Energy Storage, 46*, 103855.

[15] Patnaik, L., Praneeth, A. V. J. S., & Williamson, S. S. (2019). A Closed-Loop Constant-Temperature Constant-Voltage Charging Technique to Reduce Charge Time of Lithium-Ion Batteries. *IEEE Transactions on Industrial Electronics*, *66*(5), 1059-1067.

[16] Fu, Z., Fan, Y., Cai, X., Zheng, Z., Xue, J., & Zhang, K. (2018). Lithium Titanate Battery Management System Based on MPPT and Four-Stage Charging Control for Photovoltaic Energy Storage. *Applied Sciences*, *8*(12), 2520.

[17] Dang, G., Zhang, M., Min, F., Zhang, Y., Zhang, B., Zhang, Q., Wang, J., Zhou, Y., Liu, W., Xie, J., & Mao, S. S. (2023). Lithium titanate battery system enables hybrid electric heavy-duty vehicles. *Journal of Energy Storage*, *74*, 109313.

[18] Xie, J., Wei, X., Bo, X., Zhang, P., Chen, P., Hao, W, & Yuan, M. (2023). State of charge estimation of lithium-ion battery based on extended Kalman filter algorithm. *Frontiers in Energy Research*, *11*, 1180881.

[19] Awelewa, A., Omiloli, K., Samuel, I., Olajube, A., & Popoola, O. (2023). Robust hybrid estimator for the state of charge of a lithium-ion battery. *Frontiers in Energy Research*, *10*, 1069364.

[20] Madani, S. S., Schaltz, E., Knudsen Kær, S. (2019) An Electrical Equivalent Circuit Model of a Lithium Titanate Oxide Battery. *Batteries, 5,* 31.

[21] Sarda, J., Patel, H., Popat, Y., Hui, K. L., & Sain, M. (2023). Review of Management System and State-of-Charge Estimation Methods for Electric Vehicles. *World Electric Vehicle Journal*, *14*, 325.

[22] Girijaprasanna, T., Dhanamjayulu, C. (2022). A Review on Different State of Battery Charge Estimation Techniques and Management Systems for EV Applications. *Electronics, 11*, 1795.

[23] Omiloli, K., Awelewa, A., Samuel, I., Obiazi, O., & Katende, J. (2023). State of charge estimation based on a modified extended Kalman filter. *International Journal of Electrical and Computer Engineering (IJECE)*, *13*(5), 5054-5065.

[24] Ghaeminezhad, N., & Monfared, M. (2022). Charging control strategies for lithium-ion battery packs: Review and recent developments. *IET Power Electronics*, *15*, 349–367.

[25] Salazar, D., & Garcia, M. (2022). Estimation and Comparison of SoC in Batteries Used in Electromobility Using the Thevenin Model and Coulomb Ampere Counting. *Energies*, *15*, 7204.

[26] Singirikonda, S., & Obulesu, Y. P. (2020). Battery modelling and state of charge estimation methods for Energy Management in Electric Vehicle – A review. *IOP Conference Series: Materials Science and Engineering*, *937*(1), 012046.

[27] Pavković, D., Lobrović, M., Hrgetić, M., Komljenović, A., & Smetko, V. (2014). Battery Current and Voltage Control System Design with Charging Application. In *Proceedings of 2014 IEEE Multi-Conference on Systems and Control* (pp. 1133–1138).

[28] Szumanowski, A., & Chang, Y. (2008). Battery Management System Based on Battery Nonlinear Dynamics Modeling. *IEEE Transactions on Vehicular Technology*, *57*(3), 1425 – 1432.

[29] Kvaternik, K., Pavković, D., Kozhushko, Y., & Cipek, M. (2022). Extended Kalman Filter Design for State-of-Charge Estimation of a Lithium-Titanate Battery Cell. In *Proceedings of the 2022 International Conference on Smart Systems and Technologies (SST)* (pp. 249–254).

[30] Namor, E., Torregrossa, D., Sossan, F., Cherkaoui, R., & Paolone, M. (2016). Assessment of battery ageing and implementation of an ageing aware control strategy for a load leveling application of a lithium titanate battery energy storage system. In *Proceedings of 2016 IEEE 17th Workshop on Control and Modeling for Power Electronics (COMPEL)* (pp. 1-6).

[31] Pavković, D., Premec, A., Krznar, M., & Cipek, M. (2022). Current and voltage control system designs with EKF-based state-of-charge estimator for the purpose of LiFePO4 battery cell charging. *Optimization and Engineering*, *23*, 2235-2263.

[32] Lin, Q., Wang, J., Xiong, R., Shen, W., & He, H. (2019). Towards a smarter battery management system: A critical review on optimal charging methods of lithium-ion batteries. *Energy*, *183*, 220-234.

[33] Banguero, E., Correcher, A., Pérez-Navarro, Á., Morant, F., & Aristizabal, A. (2018). A Review on Battery Charging and Discharging Control Strategies: Application to Renewable Energy Systems. *Energies*, *11*(4), 1021.

[34] Tomaszewska, A., Chu, Z., Feng, X., O'Kane, S., Liu, X., Chen, J., Ji, C., Endler, E., Li, R., Liu, L., Li, Y., Zheng, S., Vetterlein, S., Gao, M., Du, J., Parkes, M., Ouyang, M., Marinescu, M., Offer, G., & Wu, B. (2019). Lithium-ion battery fast charging: A review. *eTransportation*, *1*, 100011.

[35] Gao, Y., Zhang, X., Cheng, Q., Guo, B., & Yang, J. (2019). Classification and Review of the Charging Strategies for Commercial Lithium-Ion Batteries. *IEEE Access*, *7*, 43511-43524.

[36] Hsieh, G.-C., Chen, L.-R., & Huang, K.-S. (2001). Fuzzy-Controlled Li-Ion Battery Charge System with Active State-of-Charge Controller. *IEEE Transactions on Industrial Electronics*, *48*(3), 585-593.

[37] Vo, T.T., Chen, X., Shen, W., & Kapoor, A. (2015). New charging strategy for lithium-ion batteries based on the integration of Taguchi method and state of charge estimation. *Journal of Power Sources*, *273*, 413-422.

[38] Zou, C., Hu, X., Wei, Z., Wik, T., & Egardt, B. (2018). Electrochemical Estimation and Control for Lithium-Ion Battery Health-Aware Fast Charging. *IEEE Transactions on Industrial Electronics*, *65*(8), 6635-6645.

[39] Zou, C., Hu, X., Wei, Z., & Tang, X. (2017) Electrothermal dynamics-conscious lithium-ion battery cell-level charging management via state-monitored predictive control, *Energy, 141*, 250-259.

[40] Jiang, J., Liu, Q., Zhang, C., & Zhang, W. (2014). Evaluation of Acceptable Charging Current of Power Li-Ion Batteries Based on Polarization Characteristics. *IEEE Transactions on Industrial Electronics*, *61*(12), 6844-6851.

[41] Abdel-Monem, M., Trad, K., Omar, N., Hegazy, O., Van den Bossche, P., & Van Mierlo, J. (2017). Influence analysis of static and dynamic fast-charging current profiles on ageing performance of commercial lithium-ion batteries. *Energy*, *120*, 171-191.

[42] Lee, K.-T., Dai, M.-J., & Chuang, C.-C. (2018). Temperature-Compensated Model for Lithium-Ion Polymer Batteries with Extended Kalman Filter State-of-Charge Estimation for an Implantable Charger. *IEEE Transactions on Industrial Electronics*, *65*(1), 589-596.

[43] Rai, R., Gaglani, M., Das, S., & Panigrahi, T. (2020). Multi-Level Constant Current Based Fast Li-Ion Battery Charging Scheme with LMS Based Online State of Charge Estimation. In *Proceedings of 2020 IEEE Kansas Power and Energy Conference (KPEC 2020)*. Manhattan, KS, USA.

[44] Jiang, L., Huang, Y., Li, Y., Yu, J., Qiao, X., Huang, C., Cao, Y. (2021) Optimization of Variable-Current Charging Strategy Based on SOC Segmentation for Li-ion Battery, *IEEE Transactions on Intelligent Transportation Systems, 22*(1), 622-629.

[45] Chen, Z., Xia, B., Mi, C. C., & Xiong, R. (2015). Loss-Minimization-Based Charging Strategy for Lithium-Ion Battery. *IEEE Transactions on Industry Applications*, *51*(5), 4121-4129.

[46] Wassiliadis, N., Schneider, J., Frank, A., Wildfeuer, L., Lin, X., Jossen, A., & Lienkamp, M. (2021). Review of fast charging strategies for lithium-ion battery systems and their applicability for battery electric vehicles. *Journal of Energy Storage*, *44*, 103306.

[47] Al-Saadi, M., Olmos, J., Saez-de-Ibarra, A., Van Mierlo, J., & Berecibar, M. (2022). Fast Charging Impact on the Lithium-Ion Batteries' Lifetime and Cost-Effective Battery Sizing in Heavy-Duty Electric Vehicles Applications. *Energies*, *15*(4), 1278.

[48] Thakur, A. K., Sathyamurthy, R., Velraj, R., Saidur, R., Pandey, A. K., Ma, Z., Singh, P., Hazra, S., K., Sharshir, S. W., Prabakaran, R., Chul Kim, S., Panchal, S., & Ali, H. M. (2023). A state-of-the art review on advancing battery thermal management systems for fast-charging. *Applied Thermal Engineering*, *226*, 120303.

[49] Ceraolo, M. (2000). New Dynamical Models of Lead-Acid Batteries. *IEEE Transactions on Power Systems*, *15*(4), 1184-1190.

[50] https://shop.gwl.eu/LTO-technology/Cylindrical-Lithium-Titanate-Oxid-Battery-Cell-LTO-2-3V-30AH.html (Accessed 9.2.2024.)

[51] Kvaternik, K., Pavković, D., Kozhushko, Y., Cipek, M., & Krznar, M. (2023). Lithium-Titanate Battery Cell Experimental Identification and State-of-Charge Estimator Design. In *Proceedings of the 18th Conference on Sustainable Development of Energy, Water, and Environment Systems* (Paper No. 0036). Dubrovnik, Croatia.

[52] Ljung, L. (1987). *System identification – theory for the user*. Prentice Hall

[53] Ross, T.J. (2004). *Fuzzy Logic with Engineering Applications*. Chichester, UK: John Wiley & Sons.

[54] Grewal, M.S., & Andrews, A.P. (2001). *Kalman filtering – theory and practice*. John Wiley and Sons Ltd.

[55] Pavković, D., Krznar, M., Komljenović, A., Hrgetić, M., & Zorc, D. (2017). Dual EKF-based State and Parameter Estimator for a $LiFePO_4$ Battery Cell. *Journal of Power Electronics*, *17*(2), 398-410.

[56] STMicroelectronics: 32-bit Arm® Cortex®-M7 480MHz MCUs. Data Sheet No. DS12110 Rev 10, 2023. https://www.st.com/content/st_com/en/arm-32-bit-microcontrollers/arm-cortex-m7.html (Accessed 19.7.2024.)

[57] Arduino® GIGA R1 WiFi. Reference Manual SKU ABX00063. https://store.arduino.cc/products/giga-r1-wifi (Accessed 22.07.2024.)